

Deleterious Effect of Negative Capacitance on the Performance of Halide Perovskite Solar Cells

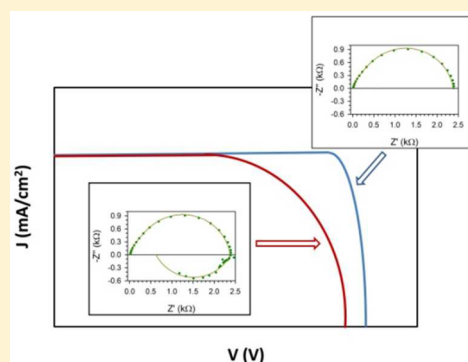
Francisco Fabregat-Santiago,^{*,†,‡} Michael Kulbak,[‡] Arava Zohar,[‡] Marta Vallés-Pelarda,[†] Gary Hodes,[‡] David Cahen,^{‡,§} and Iván Mora-Seró^{*,†,‡,§}

[†]Institute of Advanced Materials (INAM), Universitat Jaume I, 12006 Castelló, Spain

[‡]Department of Materials and Interfaces, Weizmann Institute of Science, Rehovot 76100, Israel

S Supporting Information

ABSTRACT: Negative capacitance in photovoltaic devices has been observed and reported in several cases, but its origin, at low or intermediate frequencies, is under debate. Here we unambiguously demonstrate a direct correlation between the observation of this capacitance and a corresponding decrease in performance of a halide perovskite (HaP; CsPbBr₃)-based device, expressed as reduction of open-circuit voltage and fill factor. We have prepared highly stable CsPbBr₃ HaPs that do not exhibit any degradation over the duration of the impedance spectroscopy measurements, ruling out degradation as the origin of the observed phenomena. Reconstruction of current–voltage curves from the impedance spectroscopy provided further evidence of the deleterious role of negative capacitance on photoconversion performance.



Halide perovskite (HaP)-based solar cells (HaP PV cells) constitute an intensely studied topic in photovoltaics because of the fast rise in photon to electrical energy conversion efficiencies, currently peaking at slightly above 22%.¹ In addition, the use of earth-abundant materials and of low-temperature solution-growth methods make these technologies even more attractive.^{2–5} These features have boosted interest in this topic and at the same time allowed many laboratories around the world to make such devices, owing to the relatively low cost and availability of the facilities necessary to produce them. Despite this intensive work, HaP PV cells still surprise us with unconventional behaviors. In many cases, neither the origin of these behaviors nor their influence on the final device performance are (completely) understood.

Probably the most extensively studied unconventional behavior is the hysteresis of current–potential curves^{6–13} because of its implications for determining solar cell performance.¹⁴ At the same time, preconditioning (e.g., poling, illumination) was found to affect the performance of HaP devices.^{15,16} Moreover, large capacitances have been observed at low frequencies for HaP thin films¹⁷ and have been attributed to majority carrier accumulation at the interface(s) with the contacts.¹⁸ This fact has important implications in carrier recombination, as accumulation implies a strong increase in charge density at the interfaces with consequent increase of recombination.¹⁹ Even though many aspects of these

phenomena are not completely understood, it is generally thought that ion migration plays an important role in them (even though direct proof of such migration, e.g., by isotope tracing, is still lacking).

There are other unconventional phenomena in HaPs where interpretation is not straightforward, and doubts remain concerning their origin. This is the case of the inductive loops^{20–24} and negative capacitance observed at intermediate and low frequencies by impedance spectroscopy (IS). It is likely that both phenomena would be related because both have been observed on the same sample but at different applied bias.²⁰ Nevertheless, the analysis of the relationship of both features is beyond the scope of the present Letter, which will focus instead on the negative capacitance at low frequencies. These phenomena are less-studied and less-understood than those mentioned earlier. It is worth highlighting that negative capacitance has been observed in different halide perovskite materials, with different configurations and different contacts pointing to a general behavior not reduced just to a concrete set of samples.^{17,20,25–28} The effects of this phenomenon on the performance of the HaP PV cells was not clear. In this Letter, we show that negative capacitance has, in fact, a deleterious effect on the final solar cell performance, which should provide

Received: June 25, 2017

Accepted: August 4, 2017

Published: August 4, 2017

impetus for more studies to understand this feature, because it is not just an exotic effect observed for poorly performing solar cells but is observed also in solar cells with efficiencies close to 18%.²¹

Negative capacitance at low frequencies was previously observed for non-HaP-based photovoltaic devices, such as thin-film CdS/CdTe, extremely thin absorber (ETA) solar cells, and solid-state dye-sensitized solar cells with spiro-OMeTAD as hole-transporting layer.²⁹ There are basically two different ways in the literature to interpret the negative capacitance. On one hand, it could be explained by a bulk effect, a varying series resistance of the material, which decreases under forward bias conditions.^{30,31} High injection of minority carriers at high forward bias produces the decrease of the series resistance, and this interpretation has been used to explain the observation of negative capacitance in Schottky diodes or in conventional p–n junctions.^{32–34} On the other hand, negative capacitance has been also explained by an interfacial process involving charge accumulation.³⁰ In this case, interfacial charge transfer between two media is not direct but mediated by interface states. Charge from the first medium is injected into the interfacial state and then from that state into the second medium. The kinetics of such a multistep process can produce a reduction of the interface state population, which can lead to the negative capacitance.³⁵ In that case, capacitance, defined as $C = dQ/dV$ where Q is the charge and V the voltage, becomes negative when Q decreases, because of the depopulation, while V increases. Finally, a possible relation between the electrostatic potential formed at the HaP/contact interface, due to charge accumulation in HaPs, and negative capacitance³⁶ cannot be ruled out, and it has been used recently to explain the inductive loops observed at intermediate frequencies.³⁷ We have used the term “negative capacitance” to describe this effect at low frequency because the behavior observed is similar to the one expected from a negative capacitance. We have kept this name because we think that it gives a clear image of the phenomena although the physical origin is still unclear.

Very recently we observed an increase in negative capacitance in HaPs, by the introduction of scaffolds of alternating SiO₂/TiO₂ layers, where the TiO₂ layers were not directly contacted to the extracting conductive transparent oxide; this imposes an increasing number of injection processes between the perovskite and TiO₂, leading to the conclusion that negative capacitance behavior is strongly related with the oxide/HaP interface.²⁰

The next step in understanding negative capacitance is answering the question what are the physical mechanisms causing the appearance of this behavior in HaP-based PV cells? Working toward this goal, we show here unambiguously that negative capacitance has a deleterious impact on the final PV cell performance. While we cannot yet pinpoint the physical mechanism that underlies this behavior, with the present study we hope to boost interest in this issue. The reason is that understanding (and hopefully understanding enough to prevent it) should help optimization of these devices, because, as we show, negative capacitance correlates with decrease in performance, suggesting that whatever its cause, it is harmful for PV performance.

The methodology used in this Letter to unambiguously highlight that the negative capacitance produces a deleterious effect in the solar cell performance is the direct comparison between a couple of samples where for one of them negative capacitance is observed in a broad range of applied bias, while

for the other one the range is reduced just to high applied voltages. To optimize the presentation in this Letter, we have considered that the easiest and clearest way to show this effect is by the direct comparison of just two cells prepared in the same way. However, it is important to point out that this is just an example of a completely general behavior, as we noted in above. Nevertheless, more than six samples prepared and measured in the same conditions have been analyzed, and equivalent results were found in all cases.

Current–potential (J – V) curves and impedance spectroscopy were measured for two representative different HaP PV cells (labeled as samples 1 and 2) with CsPbBr₃ as active layer and TiO₂ and poly tri-aryl amine (PTAA) as electron and hole selective layers, respectively, as described in [Experimental Methods](#). Both samples were prepared in the same way. However, there is some dispersion on the J – V curves obtained for samples from the same batch prepared in the same way, as can be observed in [Figure 1](#). To check the stability of the

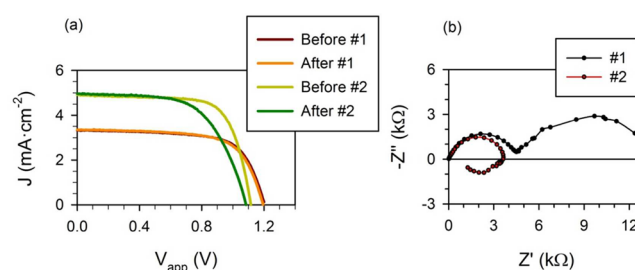


Figure 1. (a) Reverse J – V curves, scanning from positive to zero potential, showing stability of sample behavior before and after impedance measurement. See [Figure S1](#) for further examples of stability checks and [Figure S2](#) for hysteresis at reverse and forward J – V curves. (b) Representative Impedance spectra of samples 1 and 2 taken at a fixed voltage of 0.7 V and under 1 sun illumination. A prominent arc below the x -axis appears at low frequencies for sample 2.

samples during the impedance measurement, J – V curves under 1 sun illumination were recorded before and after impedance measurements. The curves registered for samples 1 and 2 are plotted in [Figure 1a](#). No difference in the recorded J – V curves is observed for sample 1 ([Figure 1a](#)), while for the sample 2, with higher current, the J – V measurement after IS measurement shows a clear loss in FF and V_{oc} although no change in the photocurrent is observed. It is well-known in the perovskite literature that the reproducibility of perovskite solar cells is limited to a certain extent. Conventionally, this reproducibility is associated with efficiency; however, other properties of the devices, such as the light soaking or poling effects, are also affected. Nevertheless, the original J – V behavior is recovered after storing the sample under dark conditions for several minutes (see [Figure S1](#) in the [Supporting Information](#)). As a result it can be concluded that the samples did not experienced any degradation during the measurement.

The Nyquist plots derived from the impedance data, [Figure 1b](#), reveal a clear difference between the two samples. While sample 1 shows two arcs, for sample 2 the second arc, due to perovskite accumulation capacitance,^{17,18} has collapsed into an arc below the x -axis (the real impedance axis Z'), which is attributed to the presence of a negative capacitance.^{29,26} In sample 2, negative capacitance arcs are seen for voltages above 0.5 V, while for sample 1 they appear only above 0.9 V and their effect is much less relevant (see [Figure S3](#) for details).

Several equivalent circuits have been used to analyze impedance spectra of HaP PV cells, but no consensus exists. Some of the elements included in these circuits have been identified (e.g., bulk capacitance C_{bulk} involved in the high-frequency arc), and their influence on the response of the solar cell was clarified. We fitted our data using an equivalent circuit that is similar to the one used previously^{20,21} but is simplified to two arc features, instead of three, for the sake of clarity (Figure 2).

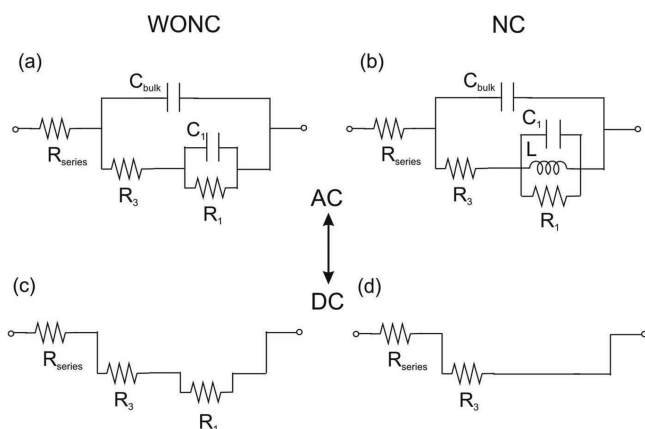


Figure 2. Equivalent circuits for AC and DC. AC circuits have been used for fitting the impedance data (a) without negative capacitance (WONC) and (b) with negative capacitance (NC). Equivalent circuits a and b are reduced to the series association of resistances at DC conditions, frequency zero, (c) WONC, as in panel a but at DC. (d) NC as in panel b but at DC when the capacitor behaves as an open circuit and inductance as a short circuit.

The equivalent circuit in Figure 2a was used to fit the experimental data for impedance spectra without negative capacitance (WONC). In this circuit, R_{series} represents the series resistance contributions of FTO, gold, contactwires, etc.; C_{bulk} represents the geometric or bulk capacitance of the film, which together with R_3 accounts for the deformed arc at high frequencies; C_1 describes the accumulation capacitance at the TiO_2 /perovskite interface and, together with R_1 (related with recombination resistance), accounts for the low-frequency arc.^{20,21} Here, we have preferred to keep the same nomenclature that was used in previous works^{20,21} to avoid renaming the elements each time, which would create confusion. We will focus on the DC resistance at frequency zero, R_{DC} , as this resistance is the inverse of the slope of the J - V curve, which is a measurement under stationary conditions (i.e., frequency zero). Consequently, when R_{DC} is known, the J - V curve can be reconstructed and the final efficiency of the solar cell can be calculated. In a Nyquist plot, R_{DC} can be obtained by the intersection with the real impedance axis of the extrapolation at zero frequency of the impedance spectra. Note that at zero frequency the impedance of a capacitor becomes infinite as $Z_C = 1/(j\omega C)$, where $j = \sqrt{-1}$ and ω is the frequency; therefore, a capacitor behaves as an open circuit. Consequently, R_{DC} for a spectrum WONC, namely hereafter $R_{\text{DC-WONC}}$, is given by the circuit in Figure 2c (the same as in Figure 2a but at zero frequency):

$$R_{\text{DC-WONC}} = R_{\text{series}} + R_3 + R_1 \quad (1)$$

When the arc below the x -axis appears, as for sample 2 in Figure 1b, data are fitted using the equivalent circuit in Figure

2b, in which the inductance is used to describe the effect of negative capacitance NC. Note that the introduction of the inductance in the circuit has an important effect on R_{DC} . The inductor impedance at zero frequency becomes zero ($Z_L = L\omega$) behaving as a short circuit, see Figure 2d (the same as in Figure 2b but at zero frequency). As a result, $R_{\text{DC-NC}}$ (R_{DC} when negative capacitance is present) is given by

$$R_{\text{DC-NC}} = R_{\text{series}} + R_3 \quad (2)$$

$R_{\text{DC-NC}}$ eliminates the influence of R_1 at zero frequency. This behavior decreases R_{DC} when negative capacitance is present. In most of the impedance analysis, just the data with positive capacitance are considered, and the existence of this low-frequency arc is typically neglected, mainly because up to now its origin and the understanding of its implications are not clear. However, negative capacitance data cannot be simply neglected, otherwise an enormous error in the determination of R_{DC} would be made (see eqs 1 and 2 and Figure 3). We show below

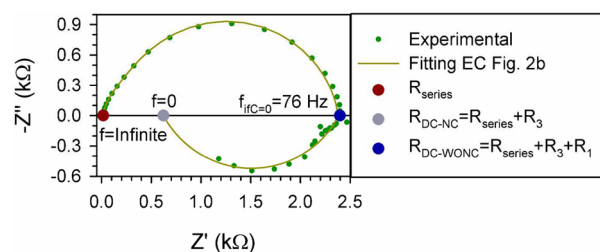


Figure 3. Impedance spectra of 2 taken at a fixed voltage of 0.8 V and under 1 sun illumination. Solid line is the fitting using the equivalent circuit, shown in Figure 2b. Different resistances and the sum of resistances are indicated on the real impedance, Z' , axis to clarify the discussion. The frequencies, f , at these Z' values, which correspond to zero capacitance, are at infinite, at intermediate, $f_{\text{ifc}=0}$, and at zero frequency (DC case).

that the negative capacitance data play a key role in the J - V curve, owing to their influence on the final value of R_{DC} and thus on the efficiency of the solar cells. Consequently, it cannot simply be removed from the analysis.

The fitting of impedance spectra using the circuits plotted in panels a and b of Figure 2 depending if the spectra is WONC or with NC, respectively, allows us to determine the values of R_{series} , R_1 , and R_3 . With these values, R_{DC} can be calculated using eq 1 or 2 depending on the case. Note that when negative capacitance is present a large error on R_{DC} can be made if $R_{\text{DC-WONC}}$ is considered instead of $R_{\text{DC-NC}}$ (see Figure 3). The DC resistance values, obtained from IS data analysis, have been used to reconstruct the J - V curves using

$$J = J_{\text{sc}} - \int_0^{V_{\text{bias}}} \frac{dV}{R_{\text{DC}}} \quad (3)$$

Considering R_{DC} obtained from the fitting (by eq 1 or 2 depending on the case) at each experimental applied bias, V_{bias} , and the short circuit current, J_{sc} , the current, J , for that corresponding bias is calculated. The pairs V_{bias} - J allow us to obtain a reconstructed (i.e., not directly measured) J - V curve. On the other hand, the real J - V curve can be directly measured by two different methods: (i) by a conventional potential scan or (ii) during an impedance measurement as current is also recorded at each applied bias. A comparison of both methods is displayed in Figure S4. Note that the second method, the measurement from impedance, is the closest one to stationary

conditions as the sample remains at the same applied voltage longer.

Taking into account these previous considerations in Figure 4, we have compared the real J - V curve obtained from

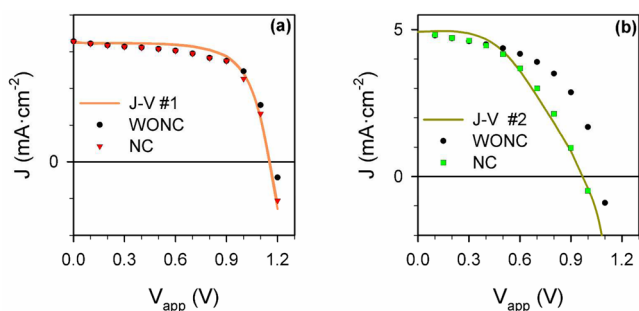


Figure 4. Real J - V curves data (lines) extracted from the direct measurement during the impedance experiment and reconstructed J - V curve (symbols) of sample 1 (a) and sample 2 (b), where the current is calculated from the R_{DC} values, obtained from fitting the impedance data with eq 3. The reconstructed J - V curves (symbols) have been calculated using $R_{DC-WONC}$ and R_{DC-NC} for each sample.

impedance measurement with the reconstructed curve where the current has been calculated with eq 3 and the R_{DC} obtained from impedance at each voltage. For each cell, two reconstructed J - V curves have been calculated using $R_{DC-WONC}$ and R_{DC-NC} (Figure 3). For sample 1, which shows negative capacitance only at the high voltages, the reconstructed J - V curve considering $R_{DC-WONC}$ (Figure 4a) presents a good agreement with the real J - V curve especially at low voltages. If the small contribution of the negative capacitance is considered by using R_{DC-NC} instead of $R_{DC-WONC}$ when the negative capacitance is observed (Figure S3), a better agreement is obtained between the real and the reconstructed curve J - V curves at high applied bias where negative capacitance is observed (Figure 4a).

For sample 2, when negative capacitance is observed at lower applied bias (Figures 1b and S3), the effect of negative capacitance on J - V is more dramatic, as shown in Figure 4b. If we do not consider the negative capacitance and consider $R_{DC-WONC}$, the reconstructed J - V curve diverges significantly from the real J - V curve. When the contribution associated with the negative capacitance is considered, by using R_{DC-NC} , the reconstructed curve matches perfectly the experimental data.

This analysis shows unambiguously on one hand that the negative capacitance cannot be simply neglected and on the other hand that the effect of the negative capacitance is critical for the performance of the solar cell, diminishing both V_{oc} and to an even higher degree the FF. However, the difference observed between these two samples is unintentional as the preparation of both cells was done in the same way. Thus, processes leading to negative capacitance and governing its magnitude are almost certainly reflecting the reproducibility problems of the preparation of HaP materials and solar cells based on them. More samples of the set have been analyzed in the same way, and similar results were obtained. Although we have analyzed a particular case, negative capacitance is a general phenomenon observed many times in HaP materials and solar cells.^{17,20,25–28}

Finally, we analyzed the effect of light intensity on the occurrence of the negative capacitance, as it is known that light produces changes in the properties of HaPs.^{17,38} Figure 5a shows the value of $f_{if C=0}$, the intermediate frequency at which the capacitance is zero (see Figure 3), under different light conditions. As illumination intensity decreases, the negative capacitance appears at lower frequencies. This result explains why normally the negative capacitance is not observed in the dark or under low illumination conditions: under these conditions, very low frequencies are needed to observe it, and at these low frequencies, the measurement is commonly very noisy and negative behavior cannot be clearly identified.

Panels b and c of Figure 5 plot both $R_{DC-WONC}$ and R_{DC-NC} obtained from impedance measurements carried out at open-circuit conditions under different light intensities for samples 1 and 2, respectively. Under these conditions, negative capacitance was observed for both samples in the 0.1–1 sun illumination range. The impedance spectra obtained at these conditions have been fitted consequently using the equivalent circuit in Figure 2b. Despite the presence of negative capacitance, both $R_{DC-WONC}$ and R_{DC-NC} have been calculated to obtain the intersection of the impedance spectra with the real impedance axis at intermediate and at zero frequency (Figure 3). This analysis allows us to determine if the weight of negative capacitance, represented by R_{DC-NC} , compared with a hypothetical sample with similar behavior but without negative capacitance, represented by $R_{DC-WONC}$, is dependent on light intensity. It can be seen in log-log representation that both samples 1 and 2 (panels b and c of Figure 5, respectively) present practically a parallel behavior. In fact, the difference in

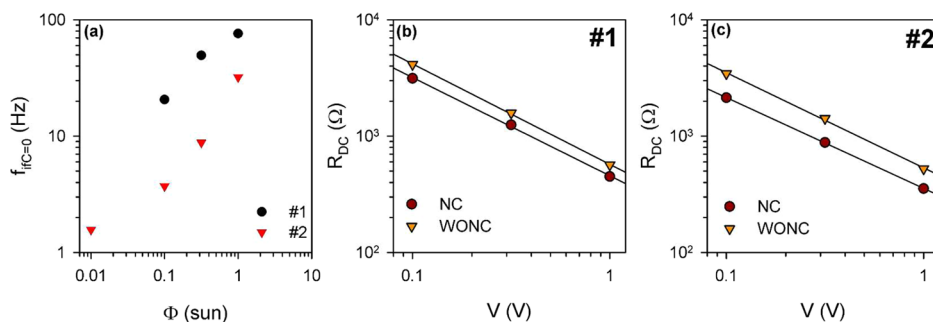


Figure 5. Impedance measurements carried out at open-circuit conditions under different light intensities. Only the cases where negative capacitance is observed are represented. (a) Intermediate frequency at which capacitance is zero, $f_{if C=0}$ (see Figure 3), and $R_{DC-WONC}$ and R_{DC-NC} calculated using eqs 1 and 2 and the values of R_{series} , R_1 , and R_3 obtained from the fitting when negative capacitance is observed (equivalent circuit 2b); (b) sample 1 and (c) sample 2. Symbols represent obtained values of $R_{DC-WONC}$ and R_{DC-NC} , while solid lines are the corresponding linear regressions.

the slopes of the linear regression of $R_{\text{DC-WONC}}$ and $R_{\text{DC-NC}}$ is less than 3% for sample 1 and less than 5% for sample 2. This finding indicates that the fraction of the negative capacitance, considering $R_{\text{DC-NC}}$ in the total impedance, considering $R_{\text{DC-WONC}}$ is independent of the illumination. An alternative way to reflect this fact is by plotting the $R_{\text{DC-WONC}}/R_{\text{DC-NC}}$ ratio, as can be observed in Figure S5.

Moreover the difference $R_{\text{DC-WONC}}$ and $R_{\text{DC-NC}}$ is higher for cell 2, with a large effect of the negative capacitance. Note that for cell 1 where the effect of negative capacitance does not cause a significant decrease of cell performance, the $R_{\text{DC-WONC}}/R_{\text{DC-NC}}$ ratio is lower than 1.5, while for sample 2 where the effect on cell performance is severe, the $R_{\text{DC-WONC}}/R_{\text{DC-NC}}$ ratio is higher than 1.5 (see Figure S5). This fact indicates that the $R_{\text{DC-WONC}}/R_{\text{DC-NC}}$ ratio can be used as a dimensionless parameter to weight the effect of negative capacitance in the cell performance.

In summary, we have shown that the presence of a negative capacitance is accompanied by a decrease of open-circuit voltage, V_{oc} , and fill factor, FF, with consequent reduction of the photoconversion efficiency of CsPbBr₃-based solar cells. We have also shown that the relative contribution of negative capacitance to total impedance is independent of the illumination but appears at lower frequencies, when illumination is reduced. The origin of the negative capacitance is not clear at this moment, and different hypotheses have been introduced: (i) variation of series resistance with the applied voltage, (ii) a multistep injection process, and (iii) formation of electrostatic potential at the interfacial accumulation region. Our recent results showing the enhancement of this negative capacitance effect with the number of interfaces²⁰ points to an important interfacial effect. Further research is needed to reveal the physical origin of this effect. The main scope of this Letter is to highlight the importance of this effect generally observed in perovskite solar cells stressing the deleterious consequences on solar cell performance. Unraveling the origin of this effect will not just help optimization of HaP-based solar cell performance but also can increase reproducibility with important implications for the field.

EXPERIMENTAL METHODS

F-doped tin oxide (FTO) transparent conducting substrates (Xinyan Technology TCO-XY15) were cut and cleaned by sequential 15 min sonication in aqueous alconox solution, deionized water, acetone, and ethanol, followed by drying under N₂ stream. After an oxygen plasma treatment for 10 min, a compact ~60 nm thin TiO₂ layer was applied to the clean substrate by spray pyrolysis of a 30 mM titanium diisopropoxidebis(acetylacetonate) (Sigma-Aldrich) solution in isopropanol using air as the carrier gas on a hot plate set to 450 °C, followed by a two-step annealing procedure at 160 and 500 °C, each for 1 h in air.

A 450 nm thick mesoporous TiO₂ scaffold was deposited by spin-coating a TiO₂ paste onto the dense TiO₂-coated substrates. A TiO₂ paste (DYESOL, DSL 18NR-T) and ethanol were mixed in a ratio of 2:7 by weight and sonicated until all the paste dissolved. The paste was spin-coated for 5 s at 500 rpm and 40 s at 2000 rpm, twice, followed by a two-step annealing procedure at 160 and 500 °C, each for 1 h in air.

The CsPbBr₃ films were prepared by a 2-step sequential deposition technique. 1 M of PbBr₂ (Sigma-Aldrich) in DMF was stirred on a hot plate at 75 °C for 20 min. It was then filtered using a 0.2 μm pore size PTFE filter and immediately

used. The solution was kept at 75 °C during the spin-coating process. The solution was spin-coated on preheated (75 °C) substrates for 30 s at 2500 rpm and was then dried on a hot plate at 70 °C for 30 min. After drying, the substrates were dipped for 10 min in a heated (70 °C) solution of 17 mg/mL CsBr (Sigma-Aldrich) in methanol for 10 min, washed with 2-propanol, dried under N₂ stream, and annealed for 10 min at 250 °C. All procedures were carried out in an ambient atmosphere. Poly[bis(4-phenyl)(2,4,6-trimethylphenyl)amine] (PTAA, Lumtec) was applied by spin-coating for 5 s at 500 rpm followed by 40 s at 2000 rpm. The PTAA solution contained 15 mg in 1 mL of chlorobenzene, mixed with 7.5 μL of 1:1 acetonitrile:*tert*-butylpyridine (TBP) solution and 7.5 μL of 170 mg/mL LiTFSi [bis(trifluoromethane)sulfonamide] in acetonitrile. The samples were left overnight in the dark in dry air before ~100 nm gold contacts were thermally evaporated on the back through a shadow mask with 0.24 cm² rectangular holes.

Current–potential curves and impedance spectroscopy were performed using a PGSTAT-30 Autolab potentiostat. *J*–*V* curves of the HaPPV cells were measured under simulated 1 sun conditions (100 mW·cm⁻², AM1.5G) using a 150 W Xe lamp. The scan rate for recording the *J*–*V* curves was 50 mV/s. For IS measurements, a 20 mV voltage AC perturbation was applied on top of the DC forward bias, which varied between 0 and 1.2 V, with the AC frequency ranging between 1 MHz and 0.05 Hz. In order to obtain the *J*–*V* curve from impedance, we have taken the value of the current at the lowest frequencies (i.e., 0.05 Hz). This allows the sample to reach the closest possible state to stationary conditions. In any case, no significant difference between the current recorded at different frequencies for the same applied bias was found. Zview software was used for the fitting of the IS spectra to the proposed equivalent circuits.

ASSOCIATED CONTENT

Supporting Information

The Supporting Information is available free of charge on the ACS Publications website at DOI: 10.1021/acsenerylett.7b00542.

J–*V* curves to highlight stability; *J*–*V* curves to show hysteresis; *J*–*V* curves before, during, and after the impedance measurements and current density's stability at the maximum power point; and impedance data at different applied voltages and $R_{\text{WONC}}/R_{\text{DC-NC}}$ ratios (PDF)

AUTHOR INFORMATION

Corresponding Authors

*E-mail: fabresan@uji.es.

*E-mail: sero@fca.uji.es.

ORCID

Francisco Fabregat-Santiago: 0000-0002-7503-1245

David Cahen: 0000-0001-8118-5446

Iván Mora-Seró: 0000-0003-2508-0994

Notes

The authors declare no competing financial interest.

ACKNOWLEDGMENTS

The work was supported by MINECO of Spain (project MAT2016-76892-C3-1-R) by Generalitat Valenciana (Project

PROMETEOII/2014/020) and by University Jaume I (Project UJIB2016-35). For work at the Weizmann Institute, partial support from the Israel Ministry of Science's Tashtiot program is gratefully acknowledged. D.C. holds the Sylvia and Rowland Schaefer Chair in Energy Research. I.M.-S. acknowledges Weizmann Institute for supporting him with a fellowship at the Institute.

REFERENCES

- (1) Yang, W. S.; Park, B.-P.; Jung, E. H.; Jeon, N. J.; Kim, Y. C.; Lee, D. U.; Shin, S. S.; Seo, J.; Kim, E. K.; Noh, J. H.; Seok, S. I. Iodide Management in Formamidinium-Lead-Halide-Based Perovskite Layers for Efficient Solar Cells. *Science* **2017**, *356*, 1376–1379.
- (2) Yang, W. S.; Noh, J. H.; Jeon, N. J.; Kim, Y. C.; Ryu, S.; Seo, J.; Seok, S. I. High-Performance Photovoltaic Perovskite Layers Fabricated through Intramolecular Exchange. *Science* **2015**, *348*, 1234–1237.
- (3) Jeon, N. J.; Noh, J. H.; Yang, W. S.; Kim, Y. C.; Ryu, S.; Seo, J.; Seok, S. I. Compositional Engineering of Perovskite Materials for High-Performance Solar Cells. *Nature* **2015**, *517*, 476–480.
- (4) Saliba, M.; Matsui, T.; Seo, J.-Y.; Domanski, K.; Correa-Baena, J.-P.; Nazeeruddin, M. K.; Zakeeruddin, S. M.; Tress, W.; Abate, A.; Hagfeldt, A.; et al. Cesium-Containing Triple Cation Perovskite Solar Cells: Improved Stability, Reproducibility and High Efficiency. *Energy Environ. Sci.* **2016**, *9*, 1989–1997.
- (5) Bi, D.; Tress, W.; Dar, M. I.; Gao, P.; Luo, J.; Renevier, C.; Schenk, K.; Abate, A.; Giordano, F.; Correa Baena, J.-P.; et al. Efficient Luminescent Solar Cells based on Tailored Mixed-Cation Perovskites. *Sci. Adv.* **2016**, *2*, e1501170.
- (6) Meloni, S.; Moehl, T.; Tress, W.; Franckevicius, M.; Saliba, M.; Lee, Y. H.; Gao, P.; Nazeeruddin, M. K.; Zakeeruddin, S. M.; Rothlisberger, U. Ionic Polarization-Induced Current-Voltage Hysteresis in $\text{CH}_3\text{NH}_3\text{PbX}_3$ Perovskite Solar Cells. *Nat. Commun.* **2016**, *7*, 10334.
- (7) Levine, I.; Nayak, P. K.; Wang, J. T.-W.; Sakai, N.; van Reenen, S.; Brenner, T. M.; Mukhopadhyay, S.; Snaith, H. J.; Hodes, G.; Cahen, D. Interface-Dependent Ion Migration/Accumulation Controls Hysteresis in MAPbI_3 Solar Cells. *J. Phys. Chem. C* **2016**, *120*, 16399–16411.
- (8) Chen, B.; Yang, M.; Priya, S.; Zhu, K. Origin of J–V Hysteresis in Perovskite Solar Cells. *J. Phys. Chem. Lett.* **2016**, *7*, 905–917.
- (9) Tress, W.; Marinova, N.; Moehl, T.; Zakeeruddin, S. M.; Nazeeruddin, M. K.; Grätzel, M. Understanding the Rate-Dependent J–V Hysteresis, Slow Time Component, and Aging in $\text{CH}_3\text{NH}_3\text{PbI}_3$ Perovskite Solar Cells: the Role of a Compensated Electric Field. *Energy Environ. Sci.* **2015**, *8*, 995–1004.
- (10) Almora, O.; Zarazua, I.; Mas-Marza, E.; Mora-Sero, I.; Bisquert, J.; Garcia-Belmonte, G. Capacitive Dark Currents, Hysteresis, and Electrode Polarization in Lead Halide Perovskite Solar Cells. *J. Phys. Chem. Lett.* **2015**, *6*, 1645–1652.
- (11) Almora, O.; Aranda, C.; Zarazua, I.; Guerrero, A.; Garcia-Belmonte, G. Noncapacitive Hysteresis in Perovskite Solar Cells at Room Temperature. *ACS Energy Lett.* **2016**, *1*, 209–215.
- (12) Unger, E. L.; Hoke, E. T.; Bailie, C. D.; Nguyen, W. H.; Bowring, A. R.; Heumüller, T.; Christoforo, M. G.; McGehee, M. D. Hysteresis and Transient Behavior in Current-Voltage Measurements of Hybrid-Perovskite Absorber Solar Cells. *Energy Environ. Sci.* **2014**, *7*, 3690–3698.
- (13) Snaith, H. J.; Abate, A.; Ball, J. M.; Eperon, G. E.; Leijtens, T.; Noel, N. K.; Stranks, S. D.; Wang, J. T.-W.; Wojciechowski, K.; Zhang, W. Anomalous Hysteresis in Perovskite Solar Cells. *J. Phys. Chem. Lett.* **2014**, *5*, 1511–1515.
- (14) Christians, J. A.; Manser, J. S.; Kamat, P. V. Best Practices in Perovskite Solar Cell Efficiency Measurements. Avoiding the Error of Making Bad Cells Look Good. *J. Phys. Chem. Lett.* **2015**, *6*, 852–857.
- (15) Xiao, Z.; Yuan, Y.; Shao, Y.; Wang, Q.; Dong, Q.; Bi, C.; Sharma, P.; Gruverman, A.; Huang, J. Giant Switchable Photovoltaic Effect in Organometal Trihalide Perovskite Devices. *Nat. Mater.* **2015**, *14*, 193–198.
- (16) O'Regan, B. C.; Barnes, P. R. F.; Li, X.; Law, C.; Palomares, E.; Marin-Beloqui, J. M. Optoelectronic Studies of Methylammonium Lead Iodide Perovskite Solar Cells with Mesoporous TiO_2 : Separation of Electronic and Chemical Charge Storage, Understanding Two Recombination Lifetimes, and the Evolution of Band Offsets during J–V Hysteresis. *J. Am. Chem. Soc.* **2015**, *137*, 5087–5099.
- (17) Juarez-Perez, E. J.; Sanchez, R. S.; Badia, L.; Garcia-Belmonte, G.; Kang, Y. S.; Mora-Sero, I.; Bisquert, J. Photoinduced Giant Dielectric Constant in Lead Halide Perovskite Solar Cells. *J. Phys. Chem. Lett.* **2014**, *5*, 2390–2394.
- (18) Zarazua, I.; Bisquert, J.; Garcia-Belmonte, G. Light-Induced Space-Charge Accumulation Zone as Photovoltaic Mechanism in Perovskite Solar Cells. *J. Phys. Chem. Lett.* **2016**, *7*, 525–528.
- (19) Zarazua, I.; Han, G.; Boix, P. P.; Mhaisalkar, S.; Fabregat-Santiago, F.; Mora-Seró, I.; Bisquert, J.; Garcia-Belmonte, G. Surface Recombination and Collection Efficiency in Perovskite Solar Cells from Impedance Analysis. *J. Phys. Chem. Lett.* **2016**, *7*, 5105–5113.
- (20) Anaya, M.; Zhang, W.; Hames, B. C.; Li, Y.; Fabregat-Santiago, F.; Calvo, M. E.; Snaith, H. J.; Míguez, H.; Mora-Sero, I. Electron Injection and Scaffold Effects in Perovskite Solar Cells. *J. Mater. Chem. C* **2017**, *5*, 634–644.
- (21) Guerrero, A.; Garcia-Belmonte, G.; Mora-Sero, I.; Bisquert, J.; Kang, Y. S.; Jacobsson, T. J.; Correa-Baena, J.-P.; Hagfeldt, A. Properties of Contact and Bulk Impedances in Hybrid Lead Halide Perovskite Solar Cells Including Inductive Loop Elements. *J. Phys. Chem. C* **2016**, *120*, 8023–8032.
- (22) Juarez-Perez, E. J.; Wußler, M.; Fabregat-Santiago, F.; Lakus-Wollny, K.; Mankel, E.; Mayer, T.; Jaegermann, W.; Mora-Sero, I. Role of the Selective Contacts in the Performance of Lead Halide Perovskite Solar Cells. *J. Phys. Chem. Lett.* **2014**, *5*, 680–685.
- (23) Contreras, L.; Idigoras, J.; Todinova, A.; Salado, M.; Kazim, S.; Ahmad, S.; Anta, J. A. Specific Cation Interactions as the Cause of Slow Dynamics and Hysteresis in Dye and Perovskite Solar Cells: a Small-Perturbation Study. *Phys. Chem. Chem. Phys.* **2016**, *18*, 31033–31042.
- (24) Wang, P.; Shao, Z.; Ulfa, M.; Pauporté, T. Insights into the Hole Blocking Layer Effect on the Perovskite Solar Cell Performance and Impedance Response. *J. Phys. Chem. C* **2017**, *121*, 9131–9141.
- (25) Dualeh, A.; Moehl, T.; Tétreault, N.; Teuscher, J.; Gao, P.; Nazeeruddin, M. K.; Grätzel, M. Impedance Spectroscopic Analysis of Lead Iodide Perovskite-Sensitized Solid-State Solar Cells. *ACS Nano* **2014**, *8*, 362–373.
- (26) Zohar, A.; Kedem, N.; Levine, I.; Zohar, D.; Vilan, A.; Ehre, D.; Hodes, G.; Cahen, D. Impedance Spectroscopic Indication for Solid State Electrochemical Reaction in $(\text{CH}_3\text{NH}_3)\text{PbI}_3$ Films. *J. Phys. Chem. Lett.* **2016**, *7*, 191–197.
- (27) Kovalenko, A.; Pospisil, J.; Zmeskal, O.; Krajcovic, J.; Weiter, M. Ionic Origin of a Negative Capacitance in Lead Halide Perovskites. *Phys. Status Solidi RRL* **2017**, *11*, 1600418.
- (28) Tai, Q.; You, P.; Sang, H.; Liu, Z.; Hu, C.; Chan, H. L. W.; Yan, F. *Nat. Commun.* **2016**, *7*, 11105.
- (29) Mora-Seró, I.; Bisquert, J.; Fabregat-Santiago, F.; Garcia-Belmonte, G.; Zoppi, G.; Durose, K.; Proskuryakov, Y.; Oja, I.; Belaidi, A.; Dittrich, T.; et al. Implications of the Negative Capacitance Observed at Forward Bias in Nanocomposite and Polycrystalline Solar Cells. *Nano Lett.* **2006**, *6*, 640–650.
- (30) Bisquert, J. A Variable Series Resistance Mechanism to Explain the Negative Capacitance Observed in Impedance Spectroscopy Measurements of Nanostructured Solar Cells. *Phys. Chem. Chem. Phys.* **2011**, *13*, 4679–4685.
- (31) Barna, A.; Horelick, D. A Simple Diode Model Including Conductivity Modulation. *IEEE Trans. Circuit Theory* **1971**, *18*, 233–240.
- (32) Lindmayer, J.; Wrigley, C. Y. *Fundamentals of Semiconductor Devices*; Van Nostrand: New York, 1965; pp 237–245, 432–449.
- (33) Laux, S. E.; Hess, K. Revisiting the Analytic Theory of p-n Junction Impedance: Improvements Guided by Computer Simulation leading to a New Equivalent Circuit. *IEEE Trans. Electron Devices* **1999**, *46*, 396–412.

(34) van den Biesen, J. J. H. Modelling the Inductive Behaviour of Short-Base p-n Junction Diodes at High Forward Bias. *Solid-State Electron.* **1990**, *33*, 1471–1476.

(35) Bisquert, J.; Garcia-Belmonte, G.; Pitarch, Á.; Bolink, H. J. Negative Capacitance caused by Electron Injection through Interfacial States in Organic Light-Emitting Diodes. *Chem. Phys. Lett.* **2006**, *422*, 184–191.

(36) Gottesman, R.; Lopez-Varo, P.; Gouda, L.; Jimenez-Tejada, J. A.; Hu, J.; Tirosh, S.; Zaban, A.; Bisquert, J. Dynamic Phenomena at Perovskite/Electron-Selective Contact Interface as Interpreted from Photovoltage Decays. *Chem.* **2016**, *1*, 776–789.

(37) Ghahremanirad, E.; Bou, A.; Olyaei, S.; Bisquert, J. Inductive Loop in the Impedance Response of Perovskite Solar Cells Explained by Surface Polarization Model. *J. Phys. Chem. Lett.* **2017**, *8*, 1402–1406.

(38) Gottesman, R.; Zaban, A. Perovskites for Photovoltaics in the Spotlight: Photoinduced Physical Changes and Their Implications. *Acc. Chem. Res.* **2016**, *49*, 320–329.